

## THE DIFFERENTIAL EMISSION MEASURE DISTRIBUTION IN THE MULTILoop CORONA

MARKUS J. ASCHWANDEN

Lockheed Martin Advanced Technology Center, Solar and Astrophysics Laboratory, Department L9-41, Building 252,  
3251 Hanover Street, Palo Alto, CA 94304; aschwanden@lmsal.com

Received 2002 September 2; accepted 2002 October 9; published 2002 October 18

### ABSTRACT

This is a rebuttal of a recent Letter on the inadequacy of temperature measurements in the solar corona through narrowband filter and line ratios by Martens et al. We simulate the differential emission measure (DEM) distribution of a multiloop corona and find that the temperature profile of individual loops can be retrieved with narrowband filter ratios. The apparently flat DEM distributions constructed from Coronal Diagnostics Spectrometer line fluxes by Schmelz et al. are an artifact of a smoothing function (in temperature), while the unsmoothed DEM distribution reveals multiple peaks of near-isothermal loops.

*Subject headings:* Sun: corona — Sun: UV radiation

### 1. INTRODUCTION

The solar corona in and around active regions consists of thousands of overdense loops, which are sporadically heated and filled with upflowing plasma. The *Transition Region and Coronal Explorer (TRACE)*, the EUV imager with the currently highest spatial resolution of  $\approx 1''$  (with pixel size of  $0''.5$ ), reveals that loop structures exist with diameters down to the instrumental resolution (Golub et al. 1999). The temperature structure of coronal loops has been investigated with three narrowband filters from *TRACE* and the *Solar and Heliospheric Observatory (SOHO)* EUV Imaging Telescope (EIT), which have their peak sensitivity at  $T \approx 1.0$  MK (171 Å),  $T \approx 1.5$  MK (195 Å), and  $T \approx 2.0$  MK (284 Å), and it was found that most of the loops have a dominant brightness in a single filter, sometimes have comparable brightness in two filters, but rarely show up co-spatially in three filters (Aschwanden et al. 1999, 2000a; Chae et al. 2002). This fact strongly suggests that loop structures, as resolved with *TRACE* down to diameters of  $\geq 1000$  km, have a single temperature in a given cross section, rather than being composed of unresolved threads with a wide range of temperatures (Testa et al. 2002). Also, the temperature variation along the loops is found to be small, on the order of  $\leq 10\%$  in the coronal segments of the loops (Neupert et al. 1998; Aschwanden et al. 1999; Lenz et al. 1999). This near isothermality can be understood in terms of hydrostatic loop models, where footpoint heating that balances radiative loss (typically with a scale height of  $s_H \approx 20$  Mm for 1 MK loops) predicts almost isothermal hydrostatic solutions (Serio et al. 1981; Schrijver et al. 1999; Aschwanden et al. 1999; Aschwanden & Schrijver 2002).

The total temperature distribution of active region loops, however, has a broad range, typically  $T \approx 1\text{--}3$  MK in the greater area around active regions or up to  $T \approx 1\text{--}8$  MK in the center of active regions (Hara et al. 1992; Kano & Tsuneta 1996). The temperature distribution can be characterized with a differential emission measure (DEM) distribution, which shows indeed a broad temperature distribution in active regions (Pallavicini, Sakurai, & Vaiana 1981; Brosius et al. 1996). Observations with narrowband EUV instruments (*TRACE*, *SOHO/EIT*) show only a narrow temperature slice in any filter, but since individual loops are near isothermal in their coronal segments, they show up as complete “semicircles” (Schrijver et al. 1999). In broadband instruments like the *Yohkoh* soft X-ray telescope (SXT) or the

future X-ray telescope on *Solar-B*, the instrument response function is increasing with temperature, and thus the hottest loops are always brightest in those images. A more complex temperature synthesis can be achieved with multiline observations from instruments like the *SOHO* Coronal Diagnostics Spectrometer (CDS). Although an instrument like CDS provides more comprehensive temperature diagnostics, it has the trade-off of multitemperature confusion along a given line of sight, which is even more severe for the relatively poor spatial resolution of CDS (although the nominal resolution is  $\approx 2''$ , the effective resolution is  $\approx 10''\text{--}15''$ , as estimated from the solar limb edge shown in Fig. 1 of Schmelz et al. 2001, where the CDS image was summed in  $4''$  pixels).

In this Letter, we simulate the DEM distribution that results in a multiloop corona and show that the near isothermality of individual loops can be recovered from such DEMs with filter-ratio methods. This simulation result questions a recent claim that narrowband filter and line ratios are inadequate for temperature measurements of coronal loops (Martens, Cirtain, & Schmelz 2002), an argument that is based on an oversimplified characterization of the multi-peaked DEM with a smooth plateau function, fitted to CDS spectral line intensities (Schmelz et al. 2001). Examining the original data of Schmelz et al. (2001), we find evidence for multiple (near co-spatial or intersecting) loops with different temperatures in the  $T \approx 1\text{--}3$  MK range that contribute to a broad-temperature DEM, rather than a single loop, as claimed by Martens et al. (2002). This study demonstrates that temperature diagnostics of coronal loops is not helped by the combination of many temperature lines alone, unless higher spatial resolution goes along with it.

### 2. MODEL SIMULATION

Our approach is to simulate a realistic DEM distribution for a coronal region above the limb. We choose an image size of  $512 \times 512$  (with pixel size of  $0''.5$ ), which corresponds to a spatial size of 185,000 km. We simulate 200 semicircular loops with random center positions in the medium 50% of the horizontal distance (Fig. 1), with a random distribution of their (logarithmic) loop half-lengths,  $\log L(\text{cm}) = 9.7 \pm 0.3$ , with a random distribution of their widths,  $\log w(\text{cm}) = 8.0 \pm 0.3$ , and a random distribution of their loop-top temperatures,

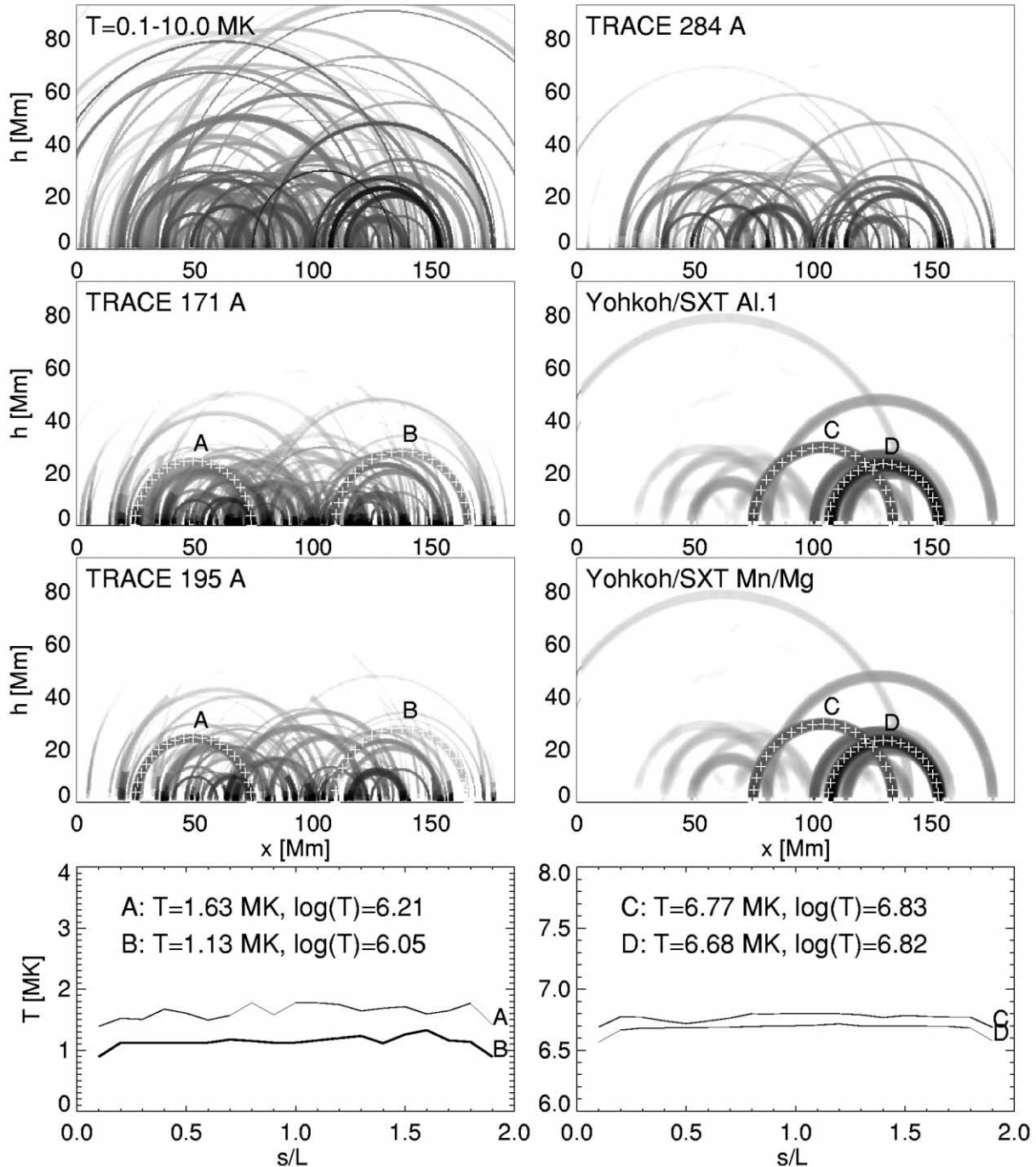


FIG. 1.—Simulation of a coronal region with 200 nested loops (*top left panel*), simulated for five instrument wave bands that are used for filter-ratio measurements. Each loop represents a hydrostatic solution, and the brightness in the image represents the DEM in each filter wave band. The brightness is logarithmic and covers a contrast of  $10^6$  for the full temperature range (*top left panel*) and  $10^3$  for each instrument wave band. Four loops are marked (A, B, C, D) for detailed DEM analysis, with the resulting filter-ratio temperatures shown in the bottom panels. The corresponding DEM distributions are shown in Fig. 2.

$\log T_{\max}(\text{K}) = 6.0 \pm 0.3$ . We calculate their temperature profiles  $T(s)$  and density profiles  $n(s)$  from hydrostatic solutions using the analytical approximations of Aschwanden & Schrijver (2002), for the case of footpoint heating with heating scale heights of  $s_H = 20$  Mm, as it was found to be most consistent with observations (Aschwanden, Nightingale, & Alexander 2000b; Aschwanden, Schrijver, & Alexander 2001). In order to obtain the DEM distributions over the entire image, we define a three-dimensional data cube  $\text{DEM}(x, y, T)$ , where the DEM

in each pixel is sampled in a logarithmic temperature range of  $\log T(\text{K}) = 5.0, \dots, 7.0$ , with logarithmic bins of  $d \log T = 0.1$ . The emission measure contributions  $d \text{EM}[x(s), y(s), T(s)] \approx n(s)^2 w$  of each of the 200 loops are accumulated in the corresponding voxels or the three-dimensional data cube  $\text{DEM}(x, y, T)$ . We simulate then five images of how they would be perceived by TRACE in the 171, 195, and 284 Å filters and by Yohkoh/SXT in Al.1 and Mn/Mg filters, by convolving the DEM data cube with the corresponding instrumental response functions

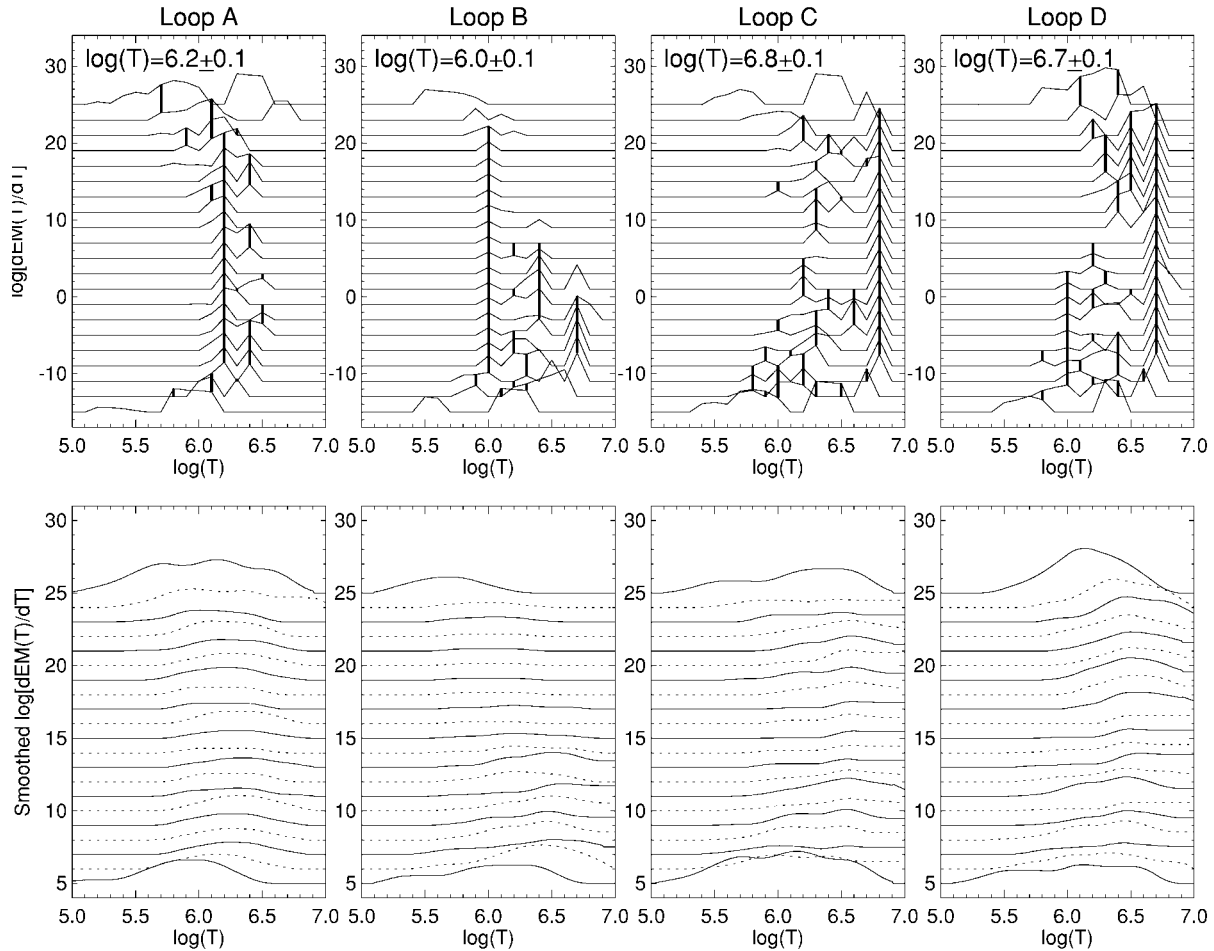


Fig. 2.—DEM distributions for the four loops (A, B, C, D) marked in Fig. 1, at 20 spatial positions each, with the  $\log dEM(T)/dT$  displaced by increments of 2 (*top*) or 1 (*bottom*) for subsequent loop positions. Isothermal loop segments are marked with thick vertical lines (*top*). The DEM curves in the bottom panels represent smoothed versions (with a boxcar of  $d \log T = 0.5$ ), similar to the CDS DEM curves shown in Schmelz et al. (2001, Fig. 6).

$R(T)$ ,

$$EM(x, y) = \int \frac{dEM(x, y, T)}{dT} R(T) dT. \quad (1)$$

The resulting images are shown in Figure 1 in gray scale, degraded with the corresponding spatial resolution of the instruments ( $1''$  for *TRACE* and  $5''$  for *SXT*). The simulated images demonstrate (1) there coexist multiple loops in most of the image pixels, which would be hard to separate with lower spatial resolution (e.g., with CDS); (2) if one singles out the brightest loop in an image, there is often a counterpart in a filter with overlapping temperature sensitivity, which makes it suitable for line-ratio techniques; and (3) loops in temperature filters with no temperature overlap are not exactly cospatial (e.g., *TRACE* 171 Å vs. *Yohkoh/SXT* Mn/Mg).

As an exercise to study the DEM of bright loops in such a multiloop environment, we mark four prominent loops that can easily be traced by eye, labeled A and B in the *TRACE* images and C and D in the *Yohkoh/SXT* images (Fig. 1, *plus signs*). We take the filter flux ratios and determine the temperatures along the loops, which are found to have the following average temperatures:  $\log T_A = 6.21$ ,  $\log T_B = 6.05$ ,  $\log T_C = 6.83$ , and  $\log T_D = 6.82$  (Fig. 1, *bottom panels*). In Figure 2, we show the DEM distributions (on a logarithmic scale) of these four loops,

A, B, C, and D, extracted at 20 positions along each loop (corresponding to the plus signs in Fig. 1). The DEM distributions along the loop coordinates  $x(s)$ ,  $y(s)$  show many near-isothermal loop segments, marked with thick vertical lines in Figure 2 (*top panels*). In spite of the confusion by cospatial (secondary) loop segments, we find for the longest (primary) loop segments A, B, C, and D the following average temperatures:  $\log T_A = 6.2 \pm 0.1$ ,  $\log T_B = 6.1 \pm 0.1$ ,  $\log T_C = 6.8 \pm 0.1$ , and  $\log T_D = 6.7 \pm 0.1$  (Fig. 2, *top panels*), which are fully consistent with the average temperatures determined from the filter-ratio technique (Fig. 1).

A CDS analysis should reveal similar, multi-peaked DEM distributions, as shown in Figure 2 (*top panels*), for a multiloop environment as simulated in Figure 1. If one smooths the multi-peaked DEMs shown in Figure 2 (*top panels*) with a boxcar of  $d \log T = 0.5$ , one suppresses the multiple peaks of individual loops with different temperatures and obtains smooth single-hump DEM distributions as shown in Figure 2 (*bottom panels*). The smoothed distributions hide the near-isothermal loops, show a broad temperature bump that is much broader than the temperature range of a single loop, and, moreover, show that the centroid of the DEM has a tendency of a higher temperature near the loop top, as expected from the *hydrostatic weighting bias* for a statistical ensemble of hydrostatic loops (Aschwanden & Nitta 2000).

## 3. DISCUSSION

The foregoing simulation should give us enough understanding of the results of a comprehensive CDS analysis, such as it has been presented by Schmelz et al. (2001), for a faint coronal loop above the limb. The line intensities of 19 CDS lines in the range from  $\log T = 5.4$  to  $\log T = 6.4$  measured at 13 loop locations (A–M) are listed in Table 1 of Schmelz et al. (2001). From the CDS response functions (shown in Fig. 4 of Schmelz et al. 2001) and numerical ratios between the line intensities and a smooth DEM curve at location H (given in Fig. 5 of Schmelz et al. 2001), we can retrieve the unsmoothed DEM distributions at each loop location A–M, which is shown in Figure 3 here. Moreover, since some temperatures are covered with multiple lines, e.g., Mg ix, Si ix, and Fe xi for  $\log T = 6.05$ , two lines for  $\log T = 6.10$ , four lines for  $\log T = 6.15$ , two lines for  $\log T = 6.20$ , and three lines for  $\log T = 6.25$  (in Table 1 of Schmelz et al. 2001), we can use the means and standard deviations from these temperatures as an estimate of the uncertainty of the  $DEM(T)/dT$  values, plotted as error bars in Figure 3. We see in Figure 3, although the DEM distribution is only plotted in temperature bins of  $d \log T = 0.1$ , that the DEM distributions are *not flat*, as claimed in Martens et al. (2002). The error bars clearly show evidence of a significant peak at  $\log T = 6.00$  over the entire loop length (A–M), a secondary peak at  $\log T = 6.10$  in the lower loop half (A–F), and a third broader bump around  $\log T \approx 6.2$ – $6.4$ . Based on the simulations shown in Figure 2 (*top panels*), we interpret these multiple peaks seen in the observed DEMs of Schmelz et al. (2001) as multiple loops or loop systems, which may be fully or partially cospatial. Using the CDS line pairs Fe xii/Fe xiv and Fe xiii/Fe xvi, where the elemental abundance cancels out, Schmelz et al. (2001) indeed report the finding of isothermal loops with temperatures of  $T = 1.64 \pm 0.07$  MK,  $\log T = 6.21$  and of  $T = 2.00 \pm 0.05$  MK,  $\log T = 6.30$  (see their Fig. 3). At any rate, the error bars of the CDS measurements clearly show that the observed DEM cannot be represented by a *smooth function*. The discrepancy between the real measured DEM and a *smoothed DEM function* is explicitly shown in the bottom of Figure 5 of Schmelz et al. (2001), with deviations by factors of 0.5–1.2, amounting to several sigmas of the formal CDS uncertainties. We suggest that these deviations from a smooth DEM function are real, and therefore they should not be smoothed out in a DEM fit, as shown in Fig. 6 of Schmelz et al. (2001), where the smoothed version of the observed DEM distribution displays a broad single hump, which has the form of a plateau near the footpoint, while the centroid shifts toward a higher temperature at the loop top, as simulated in Figure 2 (*bottom panels*).

The misleading characterization of the CDS-composed DEM distribution by a smooth function led Martens et al. (2002) to believe that the DEM distribution of a single loop is broad in temperature itself. Taking it to the extreme, they characterized the smoothed DEM distribution with a *flat plateau* between 0.7 and 2.8 MK (Fig. 1 in Martens et al. 2002) and concluded that the filter ratio in this temperature range would be constant. Consequently, they concluded that a narrowband instrument would measure a constant filter ratio along the loop and could not distinguish whether the loop is truly isothermal or composed of a broad temperature range. From our simulations shown in Figure 2 and the observed multi-peaks (Fig. 3) in the CDS-inferred DEM distribution by Schmelz et al. (2001), we conclude that the reasoning of Martens et al. (2002) is based on the misleading characterization of the observed DEM with an oversimplified smooth DEM function that forces a fit of a

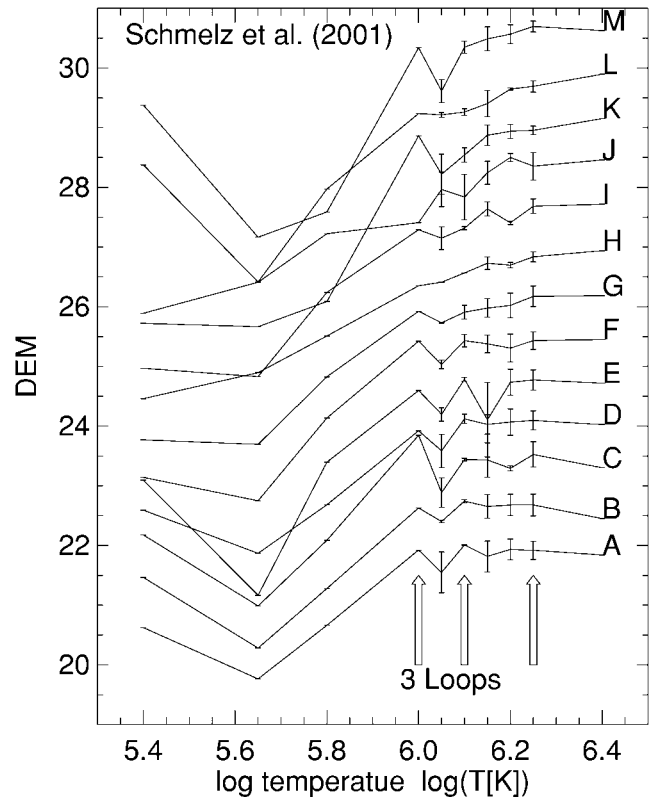


FIG. 3.—*Unsmoothed* DEM distributions of the CDS data inferred from Schmelz et al. (2001), shown for 13 loop positions A–M along the loop. Error bars are indicated when multiple lines are available at the same temperature. The *unsmoothed* DEM distributions exhibit a multi-peaked structure, indicating at least three distinct loops, which are lost in the smoothed DEM representation of Schmelz et al. (2001).

single hump over the broad temperature range of  $\log T \approx 5.7$ – $6.7$  (see Fig. 6 in Schmelz et al. 2001).

## 4. CONCLUSIONS

We simulated the DEM distributions of a multiloop corona and demonstrated that the DEM function is likely to contain multiple peaks, resulting from multiple loops along the same line of sight with different temperatures. This is true regardless of whether the different temperature loops are near cospatial or when they overlap only partially. Consequently, one should not expect a *smooth function* of the DEM distribution at any location in the corona. The CDS analysis of Schmelz et al. (2001) characterized the multi-peaked DEM distribution with an oversimplified, smoothed single-hump function, which erases the multi-peaks of individual loops and gives the misleading impression that the DEM distribution of a single loop is flat and broadband and thus would invalidate temperature measurements with narrowband filter-ratio methods (Martens et al. 2002). The apparently flat DEM distribution constructed from CDS fluxes by Schmelz et al. (2001), however, is only an artifact of a smoothing function, on which Martens's argument is based. The multiloop confusion in CDS data is particularly severe because of the relatively poor spatial resolution, while *TRACE* has a 10–15 times better spatial resolution to resolve adjacent loops and suffers much less temperature confusion by virtue of the narrowband filters. The simulation shown in Figure 2 demonstrates that the DEM is likely to show multiple subpeaks for the brightest loops, where the

filter ratio varies in two closely spaced lines ( $d \log T \approx 0.2$ ), so that the temperature profiles  $T(s)$  of individual loops can be measured by filter ratios with narrowband instruments like *TRACE* (as we demonstrated in Fig. 1), as well as with CDS for temperature-overlapping line pairs (as Schmelz et al. 2001 are reporting), in contrast to Martens's argument. Moreover, a higher spatial resolution (e.g., using *TRACE*) helps to separate closely spaced loops in the first place, in addition to the smaller tem-

perature confusion of narrowband filters. For future data analysis that will continue with CDS, *TRACE*, *Solar-B*, *STEREO*, and the Solar Dynamics Observatory, detailed modeling of the multitemperature corona is recommended to improve our observational diagnostics and physical understanding of coronal loops.

Part of this work was supported by NASA contracts NAS5-38099 (*TRACE*) and NAS8-00119 (*SXT*).

## REFERENCES

- Aschwanden, M. J., Alexander, D., Hurlburt, N., Newmark, J. S., Neupert, W. M., Klimchuk, J. A., & Gary, G. A. 2000a, *ApJ*, 531, 1129
- Aschwanden, M. J., Newmark, J. S., Delaboudiniere, J. P., Neupert, W. M., Klimchuk, J. A., Gary, G. A., Portier-Fornazzi, F., & Zucker, A. 1999, *ApJ*, 515, 842
- Aschwanden, M. J., Nightingale, R. W., & Alexander, D. 2000b, *ApJ*, 541, 1059
- Aschwanden, M. J., & Nitta, N. 2000, *ApJ*, 535, L59
- Aschwanden, M. J., & Schrijver, C. J. 2002, *ApJS*, 142, 269
- Aschwanden, M. J., Schrijver, C. J., & Alexander, D. 2001, *ApJ*, 550, 1036
- Brosius, J. W., Davila, J. M., Thomas, R. J., & Monsignori-Fossi, B. C. 1996, *ApJS*, 106, 143
- Chae, J., Park, Y. D., Moon, Y. J., Wang, H., & Yun, H. S. 2002, *ApJ*, 567, L159
- Golub, L., et al. 1999, *Phys. Plasmas*, 6(5), 2205
- Hara, H., Tsuneta, S., Lemen, J. R., Acton, L. W., & McTiernan, J. M. 1992, *PASJ*, 44, L135
- Kano, R., & Tsuneta, S. 1996, *PASJ*, 48, 535
- Lenz, D. D., DeLuca, E. E., Golub, L., Rosner, R., & Bookbinder, J. A. 1999, *ApJ*, 517, L155
- Martens, P. C. H., Cirtain, J. W., & Schmelz, J. T. 2002, *ApJ*, 577, L115
- Neupert, W. M., et al. 1998, *Sol. Phys.*, 183, 305
- Pallavicini, R., Sakurai, T., & Vaiana, G. S. 1981, *A&A*, 98, 316
- Schmelz, J. T., Scopes, R. T., Cirtain, J. W., Winter, H. D., & Allen, J. D. 2001, *ApJ*, 556, 896
- Schrijver, C. J., et al. 1999, *Sol. Phys.*, 187, 261
- Serio, S., Peres, G., Vaiana, G. S., Golub, L., & Rosner, R. 1981, *ApJ*, 243, 288
- Testa, P., Peres, G., Reale, F., & Orlando, S. 2002, *ApJ*, in press